LHCb-CONF-2012-033
November 23, 2012

Optimization and calibration of the same-side kaon tagging algorithm using hadronic B_s^0 decays in 2011 data

The LHCb collaboration[1]

Abstract

We report on the optimization and calibration of the same-side kaon tagging algorithm using the decay $B_s^0 \to D_s^- \pi^+$ with $1\,\text{fb}^{-1}$ of data from the LHCb 2011 physics run. After a data-driven optimization and calibration, we measured an effective tagging efficiency for the same-side tagger of $(1.5 \pm 0.4)\%$ using event-by-event predicted mistag for $B_s^0 \to D_s^- \pi^+$ decays. For the combination of same-side kaon and opposite-side taggers the corresponding effective tagging efficiency is $(3.8 \pm 0.7)\%$ using event-by-event predicted mistag in this channel.

[1]Prepared for the Hadron Collider Physics Symposium 2012. Contact author: Georg Krocker, krocker@physi.uni-heidelberg.de

1 Introduction

Measurements sensitive to flavour oscillations of neutral bottom mesons require, besides other inputs, the knowledge of the production and decay flavour of the reconstructed B meson (B meson indicates B^0 and B_s^0 mesons in this note). While the latter can be directly extracted from the analysis of the decay products of the B meson in flavour-specific decays, dedicated algorithms are necessary to extract the flavour at production time. At LHCb, two types of flavour tagging algorithms are in use. Opposite-side (OS) tagging algorithms rely on the pair production of b and $\bar{b}$ quarks and infer the flavour of a given B meson (signal B) from the identification of the flavour of the other b hadron (tagging B). These algorihms can be used for all signal B flavours while the same side tagging algorithms are specific for either B^0 or B_s^0. The OS taggers have been widely used in analyses at LHCb and extensive studies on their performance have been performed [1, 2, 3]. The same-side (SS) taggers on the other hand exploit the fact that in the hadronization of the signal B meson, either B^0 or B_s^0, the d and s quarks are produced in quark anti-quark pairs. While one of the quarks is used to form the neutral B meson, the other hadronizes into a pion or kaon that may be charged. The charge of this pion or kaon is determined by the flavour of its d or s quark which allows the determination of the flavour of the B meson. In case of B_s^0 mesons a charged kaon is formed in about 50% of the cases according to the simulation of fragmentation implemented in Pythia.

The study of the same-side kaon (SSK) tagging algorithm is complicated by the relatively low B_s^0 production rate. Moreover the measurement of the tagging performance requires the analysis of the fast B_s^0 mixing which implies a precise knowledge of the B_s^0 decay time resolution, σ_t. In fact the observed oscillation amplitude is directly related to the product of the dilution factors due to tagging imperfection and time resolution, $\mathcal{D}_{tag}$ and $\mathcal{D}_t$, via

$$\mathcal{A}(t) \propto \mathcal{D}_{tag}\mathcal{D}_t \cos(\Delta m_s t)/\cosh(\Delta\Gamma_s t/2) \simeq (1-2\omega)\, e^{-\frac{1}{2}(\Delta m_s \sigma_t)^2} \cos(\Delta m_s t)/\cosh(\Delta\Gamma_s t/2)\,., \quad (1)$$

where δm_s and $\Delta\Gamma_s$ are the mass difference and the decay-width difference between the heavy and light B_s^0 physical eigenstates. The performance of a tagging algorithm is determined by the effective tagging efficiency, or tagging power, $\varepsilon_{\mathit{eff}}$, that is defined by

$$\varepsilon_{\mathit{eff}} = \varepsilon_{tag}(1-2\omega)^2 = \varepsilon_{tag}\mathcal{D}_{tag}^2\,, \quad (2)$$

where the efficiency ε_{tag} and mistag fraction ω are defined as

$$\varepsilon_{tag} = \frac{R+W}{R+W+U}\,, \qquad \omega = \frac{W}{R+W}\,. \quad (3)$$

Here, R, W and U are the number of right tagged, wrong tagged and untagged candidates, respectively. The effective efficiency $\varepsilon_{\mathit{eff}} = \varepsilon_{tag}\mathcal{D}_{tag}^2$ is the figure of merit of the flavour tagging performance, which is to be maximized in the optimization procedure. In this note we present an optimization and calibration of the SSK tagger using the decay $B_s^0 \to D_s^-\pi^+$ reconstructed in $1\,\mathrm{fb}^{-1}$ of 2011 data and its combination with the OS tagging.

2 The same-side kaon tagging algorithm

The same-side kaon tagging algorithm is designed to select the charged kaons produced in the B_s^0 fragmentation by using the fact that these kaons are close to the B_s^0 in phase space while at the same time rejecting background from poorly reconstructed tracks and other particles in the event.
The flavour of the B_s^0 is determined by selecting a single fragmentation kaon (the tagging candidate) using a two step procedure. First, simulated events in which the production flavor is known are used to define a baseline set of selection criteria sensitive to the identification of the most likely fragmentation candidate. Then, the selection criteria are optimized on data in an iterative procedure that maximizes the effective tagging power determined in an analysis of the B_s^0 oscillation in the decay $B_s^0 \to D_s^-\pi^+$.

After the selection of a suitable tagging candidate, the probability of a correct tag is determined using an artificial neural network to combine several quantities of the selected tagging particle. The output is calibrated relating the knowledge of the mistag from the oscillation fit to the prediction from the neural network via a linear calibration function. Details of the procedure are given in the following.

2.1 Selection of the tagging candidate

All reconstructed tracks must satisfy minimal requirements to be considered as tagging particles, both for the SS and the OS taggers. To ensure a good track quality a cut on the track $\chi^2/d.o.f$ is applied and tracks are required to have hits in both the vertex detector and the tracking stations in front of and behind the magnet. To suppress the contamination from signal B decay products, all tracks that are explicitly contained in the decay chain are vetoed. Tagging tracks are also required to be outside a conical volume around the B direction and its decay products defined by a minimum cut on the distance in the azimuthal angle ϕ. Low momentum particles tend to be poorly reconstructed and are therefor excluded. Due to pile-up an event can contain primary vertices (PV) in addition to the one the B originated from. To eliminate contamination from other PVs in the event, the tagging tracks are required to be significantly detached from any other PV. Maximum momentum and transverse momentum cuts reject particles, that suffer from degraded particle identification performance. These preselection cuts are tuned on simulated events. Since they are common to all taggers we have not revisited them in the optimization of the tagging selection that is described in this note.

While the preselection is primarily designed to select tracks of good quality, the final selection aims to separate kaons that come from the b-fragmentation on the signal B_s^0 side, from kaons or other particles that originate from the opposite-side B decay or from the underlying event. Pion and proton backgrounds are suppressed using information from the RICH. Since the same-side tagging kaon comes from the primary fragmentation of the b quark, it tends to be close to the signal B_s^0 in phase space. Cuts on the maximum difference of the pseudorapidity η and the angle ϕ between the B_s^0 momentum and the tagging track select tracks close to the B_s^0 while additional cuts on the minimum momentum and transverse momentum of the tagging particle candidate reject low momentum particles from the primary interaction. An upper cut on the significance of the impact parameter IP/σ_{IP} of the tagging particle with respect to the signal B_s^0 production vertex assures that the tagging particle is coming from the signal B vertex. An upper cut on the difference in invariant mass $dQ = m(B_s^0 K) - m(B_s^0)$ reduces the contamination from non-fragmentation particles.

In case that multiple tagging particles satisfy the requirements, the one with the highest transverse momentum is selected. The tag is then determined by the charge of the selected kaon. In case no suitable kaon is found the B_s^0 is considered untagged by the same-side kaon tagger.

2.2 Predicted mistag probabilities

In addition to the tagging decision, the tagging algorithm returns the probability for the tag decision to be wrong as determined by a neural network classifier with several input variables. This neural network has been trained on simulated $B_s^0 \to D_s^- \pi^+$ signal events to identify the correct tag decision. The inputs to the neural network are the transverse momentum of the B_s^0 candidate, the transverse momentum of the selected SSK tagging track as well as the differences $\Delta\eta$ and $\Delta\phi$ with respect to the B_s^0, the mass difference dQ, the number of reconstructed PVs and the number of tagging tracks that pass the preselection cuts. Since the simulation does not fully represent the distributions in data, the predicted mistag probability η of the neural network does not necessarily correspond to the real mistag probability fraction ω and needs to be calibrated using flavour specific decays obtained from data. The calibration of the predicted mistag probability on the $B_s^0 \to D_s^- \pi^+$ sample is described later.

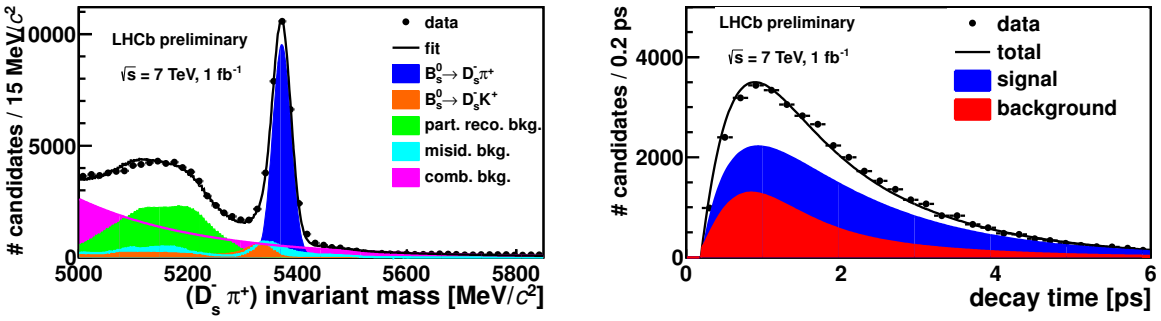

(a) mass distribution

(b) decay time distribution

Figure 1: Projection of the sum of the 3 fitted mass distributions (a) and decay time distributions (b) in $B_s^0 \to D_s^- \pi^+$ decays in the $D_s^-\ \pi^+$ invariant mass range [5.0,5.85] GeV/c^2.

3 Optimization of the tagging performance

The goal of the optimization procedure is to find a set of selection cuts that maximise the effective tagging efficiency ε_{eff}. The effective efficiency is determined from a fit to the B_s^0 decay time distribution using the measured average mistag probability ω.

3.1 Analysis strategy

This analysis closely follows the measurement of the mixing frequency Δm_s performed in summer 2011. Details of this analysis and the selection of the $B_s^0 \to D_s^- \pi^+$ candidates can be found in Ref. [4].

For a better separation of signal and background we split the sample according to the D_s^- decay topology into three different subsamples corresponding to D_s^- decays to $\phi\pi^-$, $K^{*0}K^-$ and "non resonant", i.e. events that do not belong to any of the other categories.
As a first step an unbinned maximum likelihood mass fit is performed simultaneously in all three modes in the mass range $[5.00, 5.85]\,\mathrm{GeV}/c^2$ with the same mean and width of the signal B_s^0 distribution for the three categories to get an optimal estimate of the background fractions. The background parameters are determined separately for the three modes. The sample contains 26,155 signal B_s^0 candidates in total. A projection of the sum of the three fitted mass distributions is shown in Fig. 1 (a).

As a second step we fit for the combined decay time and mass distribution with an unbinned maximum likelihood fit, where we restrict the mass range to $[m_{B_s^0} - 3\sigma$,5.85 GeV/c^2] (where $\sigma = (16.6 \pm 0.1)\,\mathrm{MeV}/c^2$ is the signal width obtained in the first step) for a simpler background treatment. In this mass range only signal, combinatorial background and B^0/Λ_b mis-ID background contribute for the three B_s^0 decay modes under study. In the full mass range there is also a large contribution from partially reconstructed physics background. The parameters of the mass term of the PDF (B_s^0 mass and width and background fractions in the different modes) are fixed to the values obtained from the previous mass fit. The parameters of the decay time term of the PDF (decay-time distribution of the combinatorial background, decay width Γ_s and mixing frequency Δm_s of the B_s^0 and mistag probability ω for signal and background components) are free to vary in the fit.

The observed B_s^0 mixing amplitude is very sensitive to the decay time resolution and the mistag fraction, as illustrated in Eq. 1. A good knowledge of the decay time resolution is therefore crucial for the correct determination of the mistag fraction. Per event uncertainties provided by the lifetime fitter are used for the determination of the decay time resolution which need to be corrected to represent the correct uncertainty estimate on data. For the purpose of this correction we performed a study of the scaling factor needed to correct the decay time uncertainty on data, using prompt D_s^+ and D^+ combined with

Decay mode	Signal yield	f_{sig}
$B_s^0 \to D_s^-(\phi\pi^-)\pi^+$	12142±134	0.91
$B_s^0 \to D_s^-(K^*K^-)\pi^+$	8407±137	0.77
$B_s^0 \to D_s^-\pi^+$ non-resonant	5606±114	0.71

Table 1: Distribution in (a) mass and (b) decay time of the $B_s^0 \to D_s^-\pi^+$ candidates used in the analysis with fit projections overlaid.

random tracks to form false B_s^0 candidates. The resulting scaling factor is $S = 1.37 \pm 0.01$. A variation of this scaling factor due to kinematic dependencies is part of the systematic cross checks discussed in Section 4.1. The size of the decay time dilution $\mathcal{D}_t$ (*cf.* Eq. 1) taking this scaling factor into account is $\mathcal{D}_t = 0.556$. Details of this procedure to determine the decay time resolution can be found in Ref. [4].

The decay time acceptance was determined on simulated events. The accuracy to which the simulation describes the real decay time acceptance observed in data is limited. Fits with different time acceptance parametrisations show stable results of the mistag fraction. Details can be found in Ref. [4].

A study of the likelihood profiles show that the error estimate of the tagging related quantities is correct. This result is confirmed also by the output of several simulated experiments. For a detailed description of the corresponding PDFs for signal and background we refer to Ref. [4]. A projection of the sum of the three fitted decay time distributions is shown in Fig. 1. Signal yields and signal fractions in the mass window $[m_{B_s} - 3\sigma, 5.85\,\mathrm{GeV}/c^2]$ are summarized in Table 1.

3.2 Optimization procedure

For the optimization we split our sample randomly in half: one subsample is used to tune the selection cuts (tuning sample), the other subsample is used to measure the tagging performance (test sample). To avoid any bias we quote the relevant tagging performances for the various steps on the test sample unless otherwise stated. The SSK selection cuts are varied iteratively on a grid of values starting from those ones that optimize the performance on simulated events. For each iteration the tagging performance is determined from the fit of the B_s^0 oscillation. During the iterations, the variables that have the largest sensitivity to $\varepsilon_{\mathit{eff}}$ are tuned first. In case more than one variable gives the same $\varepsilon_{\mathit{eff}}$, the one with the highest tagging efficiency ε_{tag} is chosen to maximize statistics. An average mistag fraction ω_{av} is used to determine the tagging power $\varepsilon_{\mathit{eff}}$. The performance of the new set of cuts is listed in Table 2. The optimization results in an enhancement of an absolute 0.5% in $\varepsilon_{\mathit{eff}}$ on the sample used for tuning and of an absolute 0.3% in $\varepsilon_{\mathit{eff}}$ on the test sample. The tagging power of the unbiased test sample is $\varepsilon_{\mathit{eff}} = 1.4 \pm 0.4$.

	ε	ω_{av}	εD^2
Test sample	16.3±0.4	35.3±2.1	1.4±0.4
Tuning sample	15.6±0.4	33.2±2.2	1.8±0.5

Table 2: Performance of the SSK tagging algorithm after optimization. An average mistag fraction ω_{av} is used in the optimization procedure.

4 Calibration of the mistag probabilities

Besides the tagging decision, the tagging algorithms provide an estimate of the probability that the decision is correct based on the output of a neural network that combines several pieces of information on the tagging particle, the event and the B_s^0 candidate. Since the neural network is trained on MC with the optimized set of cuts to identify the correct tag decision, the predicted mistag fraction η does

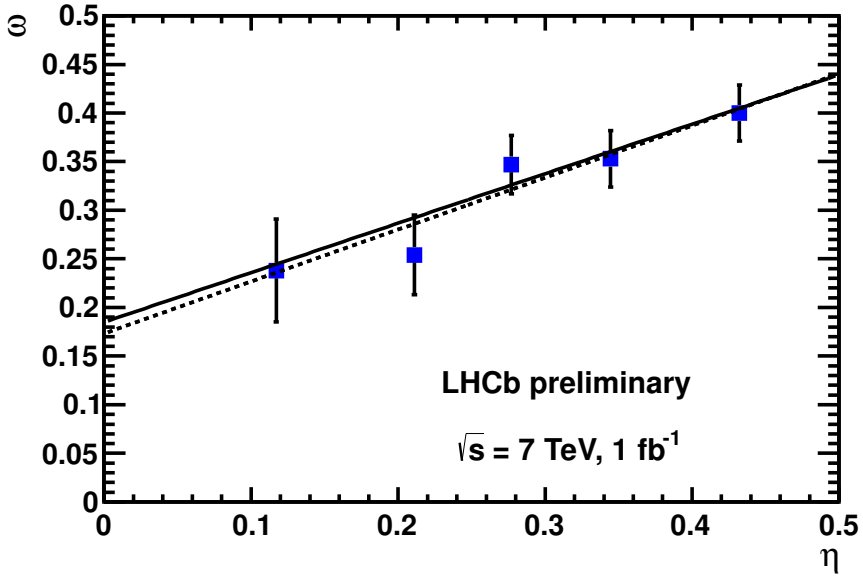

Figure 2: Average mistag fraction ω in bins of predicted mistag probability η. The solid line is the result of the unbinned fit for the calibration parameters p_0 and p_1. The dashed line is the result of a linear fit to the data points.

not necessarily correspond to the real mistag fraction ω that is measured on data and must therefore be calibrated using data. The whole sample is used to determine the calibration.

We assume a linear dependency of the measured mistag on the predicted mistag probability (η) that is parametrized as

$$\omega = p_0 + p_1 \cdot (\eta - \langle\eta\rangle) \ , \tag{4}$$

where p_0, p_1 are the calibration parameters and $\langle\eta\rangle$ is the average predicted mistag probability.

The calibration parameters p_0 and p_1 can be extracted in two ways. They can be determined directly from an unbinned maximum likelihood fit to the B_s^0 decay time distribution, where the mistag fraction ω in the decay time PDF is parametrized by the calibration function (*cf.* Eq.4). Alternatively the average mistag fraction ω can be determined in bins of the predicted mistag probability η and the results fitted using the fit function in Eq. 4 with free parameters p_0 and p_1. The results of this second approach are shown in Fig. 2, where the bins are $0 \leq \eta < 0.17$, $0.17 \leq \eta < 0.24$, $0.24 \leq \eta < 0.31$, $0.31 \leq \eta < 0.38$ and $0.38 \leq \eta$. The resulting calibration functions for both methods are shown in Fig. 2 and the calibration parameters are listed in Table 3. The correlation between the calibration parameters is $\rho(p_0, p_1) = 0.08$. The results of the two methods are in good agreement and their difference is considered as a systematic uncertainty. The result obtained by the unbinned maximum likelihood fit is taken as default. The resulting effective tagging efficiency using per-event mistag probability is $\varepsilon_{\mathit{eff}} = (1.5 \pm 0.4)\%$ in the unbiased test sample. The absolute gain with respect to using an average mistag probability is 0.1%.

4.1 Systematic uncertainties

The systematic uncertainties on the calibration parameters are determined considering several effects that can bias the calibration:

- **Flavour at production:** the initial flavour of the signal B_s^0 determines the charge of the tagging kaon. Due to the different K^+ and K^- interaction probability with matter, a dependency of the

SSK calibration	p_0	p_1	$\langle\eta\rangle$
Unbinned fit	0.350±0.015	0.51±0.16	0.3237 (fixed)
Fit of categories	0.346± 0.015	0.53±0.16	0.3237 (fixed)
Unbinned fit, calibration applied	0.349±0.015	1.00±0.30	0.3497 (fixed)

Table 3: Results of the fit of the SSK calibration parameters for an direct unbinned fit of p_0 and p_1 and of a fit in bins of the predicted mistag η. The last line shows the result for the fit if the calibration is applied.

calibration parameters on the initial flavour is possible. To determine this effect the results of three different analyses are combined: a direct measurement in $B_s^0 \to D_s^- \pi^+$, where the difference in the calibration parameter p_0 for B_s^0 and $\overline{B}_s^0$ is extracted fitting the oscillation amplitude and assuming no production asymmetry for B_s^0. The second determination is based on the dependency of the calibration parameters of the opposite-side kaon tagger on the initial B flavour that is measured in the $B^+ \to J/\psi K^+$ control channel. Finally the last result is based on the analysis of the SSK tagging calibration on prompt D_s^+ signal. A significant effect on p_0 is found. It corresponds to a smaller mistag for signal B_s^0 mesons, that are tagged by positive kaons, compared to $\overline{B}_s^0$ mesons, tagged by negative kaons. The size of the deviation is $\Delta_{p_0} = 0.01$ and has to be taken into account as systematic uncertainty. Alternatively, a correction for this difference has to be taken into account by the individual analyses using the same-side kaon tagger unless different calibration parameters are explicitely used for B_s^0 and $\overline{B}_s^0$ events.

- **Flavour at decay:** the calibration parameters are determined separately for $B_s^0 \to D_s^- \pi^+$ and $\bar{B}_s^0 \to D_s^+ \pi^-$ decays. No significative differences are found, consequently no systematic uncertainty is assigned for this effect. Due to the fast B_s^0 oscillations the asymmetries related to the different tagging performance of K^+ and K^- are washed out.

- **Charge of the tagging kaon:** possible differences on the calibration parameters related to the charge of the SS kaons are studied for samples tagged by K^+ and K^-. This approach is complementary to the direct evaluation of systematic effects due to the flavour at production time but easier to determine in the $B_s^0 \to D_s^- \pi^+$ decay. No significative differences are found, consequently no systematic uncertainty is assigned for this effect. Due to the fast B_s^0 oscillations the asymmetries related to the to different tagging performance of K^+ and K^- are washed out.

- **Fit method:** a systematic uncertainty of $\sigma_{p_0} = \pm 0.004$ and $\sigma_{p_1} = \pm 0.02$ for the difference between the results of the unbinned and the binned fits is assigned (see Section 4).

- **Decay time resolution:** the knowledge of the decay time resolution is crucial for the determination of the mistag on data. The scaling factor of the decay time resolution is determined on data using prompt D particles and random tracks to simulate fake B_s^0 candidates. We vary this scaling factor by 10% relative to account for possible dependencies on the kinematics of the B_s^0 and determine the deviation of the calibration parameters introduced by this effect to be $\sigma_{p_0} = \pm 0.006$ and $\sigma_{p_1} = \pm 0.01$.

- **Tagging behaviour of background:** as an additional cross check we studied the tagging behaviour of the background. No tagging asymmetry is observed for background sources that contribute in this mass range which is in agreement with our expectations.

- **Operational conditions dependence:** to account for possible systematic deviations related to the asymmetries of the detector efficiency, the alignment accuracy, or the variations in the data-taking conditions, the calibration parameters are determined on separate subsamples split according to the run period or the magnet polarity. No significative deviations are found, consequently no systematic uncertainty is assigned for this effect.

	σ_{p_0}	σ_{p_1}
Initial flavour	0.01	–
Fit method	0.004	0.02
Fecay time resolution	0.006	0.01
Quadratic sum	0.012	0.02
Partial quadratic sum	0.007	0.02

Table 4: Systematic uncertainties on the same-side kaon tagging calibration parameters p_0 and p_1.

Table 4 reports the sizable contributions to the systematic uncertainties and the sum in quadrature that amount to $\sigma_{p_0} = \pm 0.012$ and $\sigma_{p_1} = \pm 0.02$. In case of analyses that account for different calibrations depending on the initial flavour as for example in the analysis of $B_s^0 \to J/\psi\phi$ under study for a publication, the "flavor at production" systematic uncertainty of 0.01 should be excluded. In this case, the uncertainties in the calibration parameters are $\sigma_{p_0} = \pm 0.007$ and $\sigma_{p_1} = \pm 0.02$.

5 Validity of the calibration in other channels

Once the predicted mistag probability is calibrated on data, it can be used in the fit to the data to assign larger weights to events with low mistag probability and thus to increase the overall significance of an asymmetry measurement. A crucial point is to verify that the calibration of the SSK tagging is independent on the B_s^0 decay channel.

Since the $B_s^0 \to D_s^- \pi^+$ is the only B_s^0 calibration channel for the same-side kaon tagger with sufficient yield and a good decay time resolution, this assumption can only be checked comparing the calibration plots of different decay channels ($B_s^0 \to D_s^- \pi^+$, $B_s^0 \to J/\psi\,\phi$ and $B_s^0 \to K^+K^-$) using simulated events. In this case the calibration is performed by fitting the dependency of the true mistag, obtained knowing the true tag of the signal B_s^0, on the predicted mistag probability for events selected through the specific criteria for each analysis [5, 6].

While the distributions of the SSK predicted mistag η are different for the different channels (see Fig. 3), mainly due to different momentum distributions of the B_s^0 signal candidates, the corresponding calibrations are in agreement within the statistical uncertainty, as it is shown in Fig. 4.

6 Combination of the SSK and OS tagging

Tagged events fall into three categories: events tagged only by the OS taggers, events tagged only by the SSK and events tagged by both. The efficiency of the OS taggers is $\varepsilon = (39.6 \pm 0.3)\%$ and of the SSK $\varepsilon = (15.8 \pm 0.3)\%$. For about 6% of all signal candidates both taggers give a decision. This corresponds to roughly 16% of the OS tagged signal candidates and 40% of the SSK tagged signal candidates. For the overlap sample it is useful to combine the individual response into one decision and a corresponding predicted mistag, in order to obtain the best tagging power. In particular, since the correlations between OS and SSK taggers are expected to be negligible, the combined mistag probability η is obtained by multiplying the probabilities as explained in references [1] and [2]. The hypothesis of negligible correlation between the OS and the SSK taggers is confirmed on data and can be explained by the fact that the two taggers select complementary track samples: originating from the PV or displaced with respect to the PV in the case of the SSK and OS tagger, respectively.

The combination of the OS and SSK tagging responses relies on calibrated predicted mistags. For the SSK, the calibration found in the previous sections is applied. For the OS tagging there are two choices: either transport the calibration from the analysis of the control channel $B^+ \to J/\psi\, K^+$ ($p_0 = 0.392 \pm 0.002 \pm 0.009$ $p_1 = 1.035 \pm 0.021 \pm 0.012$ and $\langle\eta\rangle = 0.391$ [3]), or determine it using the same $B_s^0 \to D_s^- \pi^+$ sample ($p_0 = 0.412 \pm 0.011$, $p_1 = 1.14 \pm 0.13$ and $\langle\eta\rangle = 0.385$.

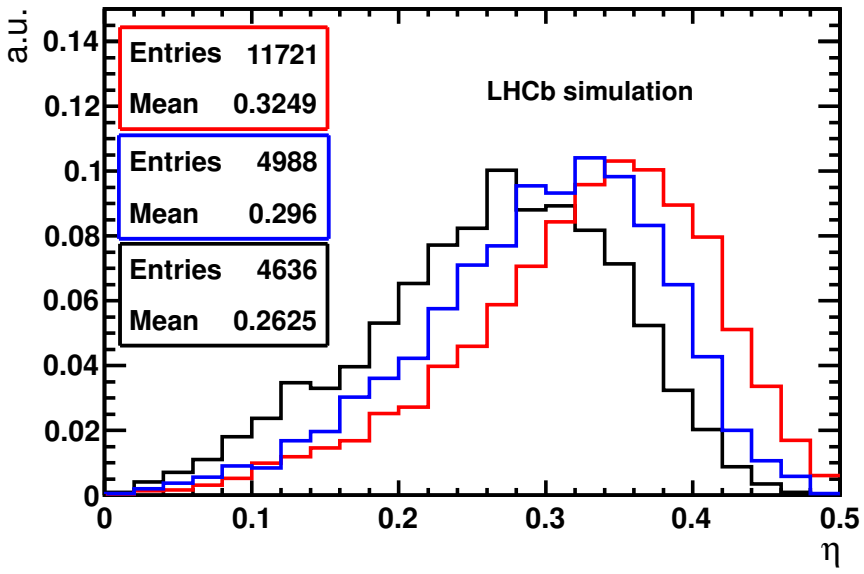

Figure 3: Distribution of the predicted mistag, η, for $B_s^0 \to D_s^- \pi^+$ (black), $B_s^0 \to K^+K^-$ (blue) and $B_s^0 \to J/\psi\,\phi$ (red) decays obtained using Monte Carlo events (histograms normalized to same unit area).

OS+SSK calibration	p_0	p_1	$\langle\eta\rangle$
Unbinned fit	0.390 ± 0.011	1.14 ± 0.13	0.3696 (fixed)
Fit in categories	0.386 ± 0.009	1.11 ± 0.11	0.3696 (fixed)
Unbinned fit, re-calibrated OST	0.391 ± 0.009	1.03 ± 0.10	0.3888 (fixed)

Table 5: Results of the fit of the calibration parameters using a direct unbinned fit of p_0 and p_1, and a fit in bins of the predicted mistag η for the combination of OS and SSK tagging. The last line shows the results of the fit in the case the OS tagger is re-calibrated using the $B_s^0 \to D_s^- \pi^+$ sample.

The results corresponding to the first choice are listed in Table 5 and Fig. 5, both for the unbinned fit and for the fit in bins of the predicted mistag, which agree perfectly. The calibration parameters are compatible within 1.9σ with the ideal values $p_0 - <\eta>= 0$ and 1.1σ for $p_1 - 1 = 0$. In this scenario the overall effective efficiency using event-by-event predicted mistag, obtained by combining the performances of the sample tagged by OS only, by SSK only and both by SSK and OS, is $\varepsilon_{\mathit{eff}} = (4.1 \pm 0.6)\%$.

The results corresponding to the second choice are also listed in Table 5 (re-calibrated OS tagger). In this scenario, the combined decision is perfectly calibrated: $p_0 - <\eta>= 0.002 \pm 0.009$ and $p_1 - 1 = 0.03 \pm 0.10$, because both OS and SSK are calibrated in the same data sample and that the two taggers are not correlated. The overall effective efficiency is $\varepsilon_{\mathit{eff}} = (3.8 \pm 0.7)\%$ on the unbiased test sample in this case.

7 Conclusion

A study of the same-side kaon tagger on $1\,\mathrm{fb}^{-1}$ of data collected by the LHCb experiment during the 2011 physics run was performed. By analysing the time dependent mixing asymmetry of the B_s^0 decays in the $B_s^0 \to D_s^- \pi^+$ control channel it was possible to optimize the performance of the same-side kaon tagger and to calibrate the predicted mistag. In particular by tuning the selection cuts of the tagging

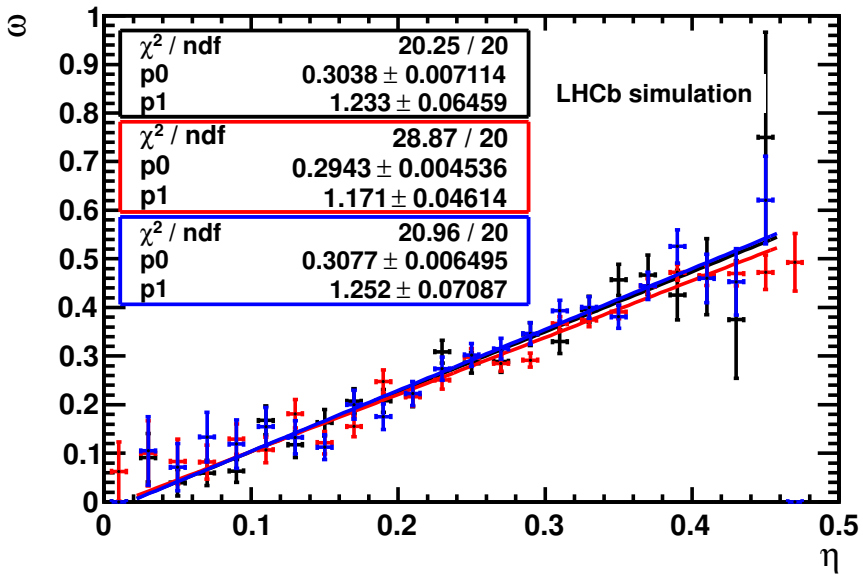

Figure 4: True mistag fraction (ω) versus predicted mistag probability (η) of simulated events of different decays: $B_s^0 \to D_s^- \pi^+$ (black), $B_s^0 \to K^+K^-$ (blue) and $B_s^0 \to J/\psi\,\phi$ (red). The results of the fit $\omega = p_0 + p_1 \cdot (\eta - \langle\eta\rangle)$ are shown.

particle, the average effective tagging power was improved by an absolute +0.3%. With the improved cuts, the first calibration of the predicted per event mistag probability was also determined. The calibration parameters are $p_0 = 0.350 \pm 0.015(\text{stat}) \pm 0.012(\text{sys})$, $p_1 = 0.51 \pm 0.16(\text{stat}) \pm 0.02(\text{sys})$ and $\langle\eta\rangle = 0.3237$, and correspond to a linear parametrization between the measured and the predicted mistag rate $\omega = p_0 + p_1(\eta - \langle\eta\rangle)$. The main systematic uncertainties are related to the dependency of the calibration parameters on the initial flavour, on the fit method and on the knowledge of B_s^0 decay time resolution. The applicability of the calibration to other B_s^0 decay channels was validated using $B_s^0 \to D_s^- \pi^+$, $B_s^0 \to J/\psi\,\phi$ and $B_s^0 \to K^+K^-$ simulated events.

The resulting same-side tagging effective efficiency is $\varepsilon_{\mathit{eff}} = (1.5 \pm 0.4)\%$, computed on the unbiased test sample, using the event-by-event predicted mistag. Using same-side kaon, opposite-side tagging and the combination of both, depending on the information available, the overall effective tagging efficiency using the event-by-event predicted mistag is $\varepsilon_{\mathit{eff}} = (3.8 \pm 0.7)\%$.

References

[1] LHCb collaboration, *Optimization and calibration of the LHCb flavour tagging performance using 2010 data*, LHCb-CONF-2011-003.

[2] LHCb collaboration, Aaij, R. and others, *Opposite-side flavour tagging of B mesons at the LHCb experiment*, Eur. Phys. J. **C72** (2012) 2022, arXiv:1202.4979.

[3] LHCb collaboration, *Performance of flavour tagging algorithms optimised for the analysis of* $B_s^0 \to J/\psi\phi$, LHCb-CONF-2012-026.

[4] LHCb collaboration, *Measurement of* Δm_s *in the decay* $B_s^0 \to D_s^-(K^+K^-\pi^-)\pi^+$ *using opposite-side and same-side flavour tagging algorithms*, LHCb-CONF-2011-050.

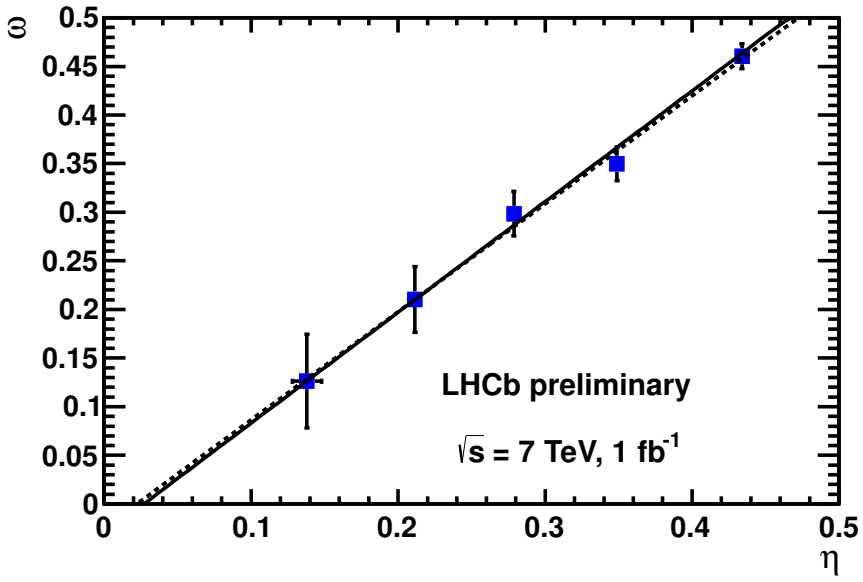

Figure 5: Average mistag fraction ω in bins of predicted mistag η of the combined (OS+SSK) taggers after calibration (OS calibration from $B^+ \to J/\psi K^+$). The solid line is the result of the unbinned fit for the calibration parameters p_0 and p_1. The dashed line is the result of a linear fit to the data points.

[5] LHCb collaboration, *Measurement of time-dependent CP violation in charmless two-body B decays*, LHCb-CONF-2012-007.

[6] LHCb collaboration, Aaij, R. and others, *Measurement of the CP-violating phase ϕ_s in the decay $B_s^0 \to J/\psi\phi$*, Phys. Rev. Lett. **108** (2012) 101803, arXiv:1112.3183.